Diagn Interv Radiol 2022; 28:83–91

MODALITY-BASED (US, CT, MRI, PET-CT) IMAGING

REVIEW

Proton density fat fraction: magnetic resonance imaging applications beyond the liver

Ilkay S. Idilman
A. Elcin Yildiz
Ali Devrim Karaosmanoglu
Mustafa N. Ozmen
Deniz Akata
Musturay Karcaaltincaba

ABSTRACT

Magnetic resonance imaging-proton density fat fraction (MRI-PDFF) is an emerging quantitative imaging biomarker that accurately measures the fat fraction of tissue by correcting factors influencing magnetic resonance signal intensity. Beyond fat quantification, it also measures R2* which is a direct measure of iron concentration. The utilization of MRI-PDFF in liver diseases is well established. In the present review, we focused on applications of MRI-PDFF in different body areas including pancreas, bone, muscle, spleen, testis, visceral, and subcutaneous adipose tissue. Future studies can enable tracking of quantitative fat fraction changes in different organs simultaneously, which can be critical in understanding the fat metabolism.

Proton density fat fraction (PDFF) derived by chemical-shift encoded magnetic resonance imaging (CSE-MRI) which is also known as magnetic resonance imaging-proton density fat fraction (MRI-PDFF) is a chemical shift-based water and fat separation technique that addresses the factors influencing magnetic resonance signal intensity in the quantitative assessment of fat.[1-3] MRI-PDFF provides accurate spectral modeling of fat and gives the ratio of the density of mobile protons from triglycerides and the total density of protons from mobile triglycerides and mobile water that reflects the concentration of mobile triglycerides within the tissue.[3] The technique allows assessment of the tissue in a short time with quantification of fat by drawing a region of interest (ROI) on the generated fat fraction maps. Iron content can also be evaluated by R2* maps obtained simultaneously with this technique. The accuracy of MRI-PDFF in quantification of hepatic fat is demonstrated in comparative studies with magnetic resonance spectroscopy[1-3] and liver biopsy.[4-6] It has also been shown to be an effective tool in the follow-up evaluation of patients with nonalcoholic fatty liver disease (NAFLD).[7,8] MRI-PDFF is also accepted as a useful biomarker to assess treatment response in the setting of early phase clinical trials in nonalcoholic steatohepatitis.[9] It has been shown to be feasible to evaluate fat accumulation in different tissues with MRI-PDFF.[10-14] In this review article, we focused on recent applications of MRI-PDFF beyond the liver including pancreas, bone marrow, muscle, spleen, testis, visceral, and subcutaneous adipose tissue.

Pancreas

The presence of fat in the pancreatic tissue has been recognized with pathology specimens and imaging modalities for decades. It was shown that MRI-PDFF is feasible in the assessment of pancreatic fat with a moderate and significant correlation with histopathologic pancreatic lipomatosis grade.[10] As a result of the assessment of the whole pancreas with this technique, fat fractions among different regions of the pancreas were also evaluated. Kühn et al.[15] observed statistically significantly different fat fractions in the pancreatic head, body, and tail with the higher fat fraction in the pancreatic body in the general population. However, other studies failed to observe such a difference in these regions.[11, 16] As a result of the variability of pancreatic fat fraction according to the positions of the ROI, Kato et al.[17] offered a 3D evaluation of pancreatic fat, which measures pancreatic fat in each slice with a freehand ROI. However, it is hard to delineate the contours of the pancreas especially in patients with atrophy or a high degree of pancreatic steatosis and interdigitating peripancreatic fat may cause potential sampling errors.

From the Department of Radiology (I.S.I., A.E.Y., A.D.K., M.N.O., D.A., M.K. ✉ *musturayk@yahoo.com*), Hacettepe University School of Medicine, Ankara, Turkey.

Received 7August 2021; revision requested 25 September 2021; last revision received 22 October 2021; accepted 26 November 2021.

Published online 22 December 2021.

DOI 10.5152/dir.2021.21845

You may cite this article as: Idilman IS, Yildiz AE, Karaosmanoglu AD, Ozmen MN, Akata D, Karcaaltincaba M. Proton density fat fraction: magnetic resonance imaging applications beyond the liver. *Diagn Interv Radiol*. 2022;28(1):83-91.

Pancreatic fat was evaluated with MRI-PDFF in various metabolic, inflammatory, and neoplastic diseases. The metabolic diseases were initially studied and research focused on metabolic associations such as NAFLD, insulin resistance, and diabetes mellitus.[11,16,18-24] Patel et al.[16] evaluated ectopic fat deposition in the pancreas and observed that MRI-determined pancreatic fat correlates with histology-determined liver steatosis grade in patients with NAFLD. In this study, researchers also observed higher pancreatic fat in patients with a NAFLD activity score higher than 5 and with no fibrosis according to the liver biopsy.[16] Idilman et al.[11] also observed slightly higher pancreatic fat in patients with hepatic steatosis and nonalcoholic steatohepatitis with no statistical significance. Several studies demonstrated a correlation between hepatic and pancreatic MRI-PDFF in patients with chronic liver disease[19] and NAFLD[18,20,21] in contrast with just one study, whose results can be explained by the limited patient number.[11]

In another study by Patel et al., [20] it was shown that patients with a higher homeostatic model assessment of insulin resistance (HOMA-IR) had higher pancreatic and liver fat (Figure 1). Idilman et al.[11] also evaluated pancreatic fat in a population of NAFLD and observed higher pancreatic fat in patients with diabetes mellitus. Sarma et al.[21] demonstrated increased liver and pancreas fat and adipose tissue in patients with type 2 diabetes mellitus. In contrast with these studies, Kühn et al.[15] compared pancreatic fat with MRI-PDFF in individuals with normal glucose tolerance, prediabetes and type 2 diabetes mellitus and observed no statistically significant differences in subgroups. There are also some studies evaluating pancreatic fat with MRI-PDFF in the pediatric and adult populations.[22, 23]

Main points

- Pancreas MRI-PDFF is shown to be related to various metabolic, inflammatory, and neoplastic diseases.
- Bone marrow MRI-PDFF allows quantification of fatty replacement which is related to loss of bone mass.
- Bone marrow MRI-PDFF determination can allow differentiation of benign fractures from malignancy-associated ones.
- Muscle MRI-PDFF can be used for the determination of muscle strength and also muscle involvement in neuromuscular diseases.

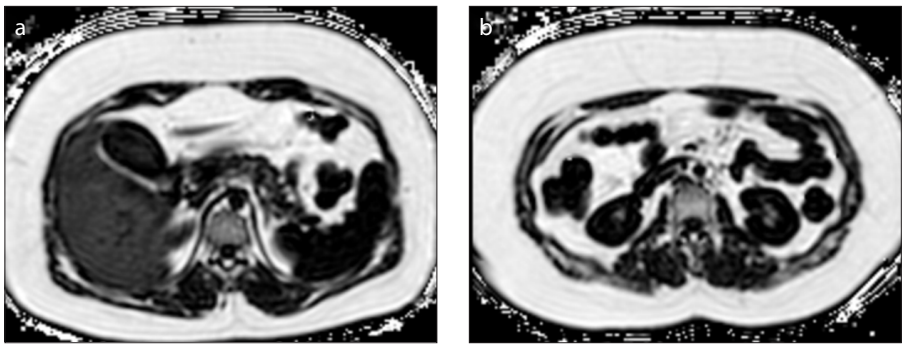

Figure 1. a, b. A 23-year-old female patient with metabolic syndrome with increased fat fraction in the liver (21.6%), pancreas (12.2%) **(a)**, lumbar vertebrae (60%), and paraspinal muscle (21.2% on the right and 18.4 % on the left) **(b)**. There is also increased VAT and SAT area **(b)**.

Trout et al.[22] observed significant correlations between pancreatic fat and patient weight, body mass index (BMI) z-score, the absolute fat area in each location of abdominal fat stores, and with midline abdominal fat thickness. In this study, the pancreatic fat fraction was not found to be a predictive factor for diabetes status.[22] However, a recent study that evaluated Chinese adolescents with obesity and NAFLD showed that liver and pancreas MRI-PDFF were both independent predictors for beta-cell dysfunction and metabolic syndrome.[23] They also showed an association between fatty pancreas and insulin resistance.[23] These results may be due to temporal changes during different stages of metabolic diseases.

There are also heterogeneous studies evaluating the relationship between pancreatic fat and different tissues and diseases as well as temporal changes. A decrease in pancreatic MRI-PDFF in accordance with the reduction in liver fat with weight loss in obese patients was observed.[24] Singh et al.[25] evaluated individuals after acute pancreatitis and observed that higher pancreatic fat depots are associated with the development of diabetes after acute pancreatitis. In another study, the authors evaluated the association between plasma metabolomics profile and liver MRI-PDFF, pancreas MRI-PDFF, and visceral adipose tissue (VAT) volume and found that two metabolites (one lysine-derivate and the bile acid conjugate taurodeoxycholate) were positively associated with pancreas PDFF which shows a possible different pathway leading to fat accumulation in the pancreas as opposed to liver and VAT[26] (Table 1). Idilman et al.[18] also demonstrated significant but weak correlations among pancreas PDFF and VAT and BMI, but no correlation was observed between pancreas PDFF and subcutaneous adipose tissue (SAT). Oguz et al.[27] evaluated pancreas PDFF in lean polycystic ovarian syndrome (PCOS) patients in comparison with healthy age and BMI matched women and observed a higher liver PDFF in the PCOS group with no difference in terms of pancreas PDFF. Despite conflicting results, a recent meta-analysis demonstrated that the presence of fatty pancreas is associated with a significantly increased risk of arterial hypertension, diabetes mellitus, and metabolic syndrome.[28] In this study, a normal pancreatic fat cutoff point of 6.2% was also suggested.[28]

Kühn et al.[15] observed that pancreatic PDFF showed a positive association with age and BMI and a negative association with serum lipase activity ($P < .001$). In accordance with this study, Kromrey et al.[29] observed significantly higher pancreatic fat content in subjects with impaired pancreatic exocrine function in comparison to subjects with normal function. They also observed an inverse correlation between pancreatic fat and fecal elastase levels. Boga et al.[30] evaluated 97 NAFLD patients and observed that increasing pancreatic steatosis is associated with a higher frequency of pancreatic exocrine insufficiency. Tahtaci et al.[31] also demonstrated a lower fecal elastase level in patients with pancreatic steatosis. Interestingly, Fukui et al.[32] observed that the pancreatic cancer patients had higher MRI-PDFF and histologic pancreatic fat fraction and in multivariate analysis, pancreas MRI-PDFF was found to be the sole independent risk factor for pancreatic cancer. These results suggest that there are complex relationships between pancreatic fat and metabolic, inflammatory, and neoplastic diseases which should comprehensively be evaluated with further studies.

Table 1. A brief summary of studies evaluating pancreas MRI-PDFF

Reference	Cohort size (n)	Cohort type	Age (years) (mean ± SD)	Methods used	Pancreas PDFF (%)	Take home points
Patel et al. [16]	43	NAFLD	N/A	1-2 ROIs were placed in pancreas head, body and tail and average was calculated	8.5 ±1.0	Increased pancreatic fat is associated with hepatic steatosis. Liver fibrosis is inversely associated with pancreatic fat content.
Idilman et al. [11]	41	NAFLD	16–67[a]	ROIs were placed in pancreas head, body and tail, average was calculated	5.7 ± 5.6	Pancreatic fat is higher in patients with type 2 DM. Patients with insulin resistance has slightly higher pancreas MRI-PDFF.
Idilman et al.[18]	135 (86/49)	Obese patients/ NAFLD	49.2 ± 11.3[b]	Each one ROI was placed in pancreas head, body and tail, average was calculated	13.2 ± 8.0	Pancreatic fat is slightly higher in patients with hepatic steatosis and nonalcoholic steatohepatitis with no statistically significance. There is a weak but significant correlation between pancreas MRI-PDFF and VAT and BMI.
Vieira et al.[19]	19/27	Chronic viral hepatitis/ chronic NALD	41.8 ± 9.7/ 45.7 ± 15.7[b]	A 6 mm ROI in pancreas head	11.5 ± 6.3	In the general study population, pancreatic PDFF values are correlated with hepatic PDFF and hepatic histologic steatosis grades. In the subgroup analyses, the correlation remained significant in patients with chronic NALD. However, patients with chronic viral hepatitis, no significant correlation was found between pancreatic and hepatic PDFF nor grades of histological liver steatosis.
Patel et al.[20]	43/49	NAFLD/healthy controls	48.4 ± 11.9/ 43.2 ± 20.0[b]	1-2 ROIs were placed in pancreas head, body and tail and average was calculated	8.5 ± 6.6/ 3.6 ± 2.3	Patients with NAFLD have higher pancreatic fat content than healthy controls. There is a significant correlation between MRI-estimated pancreatic and liver fat content amongst patients with NAFLD and healthy controls. Increased insulin resistance determined by HOMA-IR is associated with increased liver and pancreatic fat content.
Sarma et al.[21]	14/13/11	Type 2 DM/Age-matched healthy controls/young healthy controls	57.5 ± 7.2/ 58.8 ± 7.7/ 27.7 ± 2.2[b]	Pancreas were segmented using the region growing algorithm and average fat fraction was computed	5.7 (4.8–8.8)/ 4.9 (4.0–5.8)/ 4.1 (3.1–4.3)	There is a close correlation between hepatic and pancreatic PDFF. Type-2 DM is associated with increased amounts of adipose tissues and visceral fat deposits in the liver and pancreas.
Trout et al.[22]	50/21/9/6	Children/young adult population with known or suspected fatty liver disease Caucasian/Hispanic/ African American/Non-Hispanic	14.8 ± 2.7/ 11.8 ± 3.3/ 16.8 ± 3.1/ 13.3 ± 3.14[b]	ROIs were placed in the head/uncinate process and tail of the pancreas	6 ± 4/ 5 ± 5/ 5 ± 4/ 6 ± 3	Total fat area and weight are significant predictors of pancreatic fat percentage. Liver fat fraction or pancreatic fat fraction is not predictive of diabetes status.
Chiyanika et al.[23]	52	Adolescents with obesity and NAFLD	15.7 ± 1.2[b]	1 cm^2 ROIs were placed in pancreas head, body and tail thrice and average was calculated	5.3 ± 1.7	Pancreas and liver PDFF are both independent predictors of beta cells dysfunction and metabolic syndrome. Presence of fatty pancreas in obesity was associated with insulin resistance and metabolic syndrome.

Table 1. A brief summary of studies evaluating pancreas MRI-PDFF (Cont'd)

Reference	Cohort size (n)	Cohort type	Age (years) (mean ± SD)	Methods used	Pancreas PDFF (%)	Take home points
Covarrubias et al.[24]	9	Adults with severe obesity and NAFLD	28-65[a]	1 cm^2 ROIs were placed in pancreas head, body and tail and average was calculated	14.3 ± 7.9	Pancreatic PDFF decreases with dietary and surgical intervention that suggest mobilization of pancreatic fat stores during weight loss as well as hepatic PDFF, VAT, SAT and other anthropometric indices.
Singh et al.[25]	17/67/28	Adults with a history of acute pancreatitis with diabetes/without diabetes/healthy cohort	60 (51–68) / 55 (43–65)/ 45 (29 –53)[c]	Three ROIs were placed in pancreas head, body and tail and average was calculated	10.2 ± 1.2/ 9.2 ± 1.7/ 7.9 ± 1.9	Individuals after an episode of acute pancreatitis have larger visceral fat and pancreatic fat depots, which are significantly associated with the presence of diabetes after acute pancreatitis.
Lind et al.[26]	310	EFFECT I and II study participants	64.6 ± 7.2[b]	Median of the fat fraction values inside the delineated pancreas volume	10.8 ±7.7	There are several overlapping metabolomic associations between liver fat and VAT which are not shared with pancreatic fat percentage that indicates partly distinct profiles associated with different ectopic fat depots.

MRI-PDFF, magnetic resonance imaging-proton density fat fraction; SD, standard deviation; NAFLD, nonalcoholic fatty liver disease; N/A, not available; ROI, region of interest; DM, diabetes mellitus; VAT, visceral adipose tissue; BMI, body mass index; NALD, nonalcoholic liver disease; HOMA-IR, homeostatic model assessment of insulin resistance; SAT, subcutaneous adipose tissue.
[a] Range; [b] mean ± SD; [c] median (IQR).

Bone marrow

MRI-PDFF has also been used for the evaluation of the bone marrow.[12-14,33,34] It is known that bone marrow fat increases with age presumably as a result of fatty bone marrow replacement with loss of bone mass of the vertebrae.[35] The ratio of adipocytic to hematopoietic/stromal tissue is shown to be higher in osteoporotic bone in comparison with normal controls.[36] Studies evaluating lumbar vertebral MRI-PDFF in comparison with bone mineral densitometry (BMD) examination observed a statistically significant negative correlation between MRI-PDFF and BMD with higher MRI-PDFF in patients with osteopenia or osteoporosis.[12-14] Ergen et al.[13] also proposed a cutoff value of 39.2% for differentiation of osteoporotic and/or osteopenic groups from the healthy population. Guo et al.[33] evaluated the role of MRI-PDFF in combination with quantitative susceptibility mapping (QSM), which is increased with osteopenia and osteoporosis, and proposed a combination of QSM and MRI-PDFF for the assessment of postmenopausal osteoporosis. Martel et al.[34] reported a reliable assessment of proximal femur bone marrow adipose tissue quantity and composition with MRI-PDFF and validated with magnetic resonance spectroscopy. Baum et al.[37] evaluated the age-related changes in bone marrow with MRI-PDFF and observed an accelerated fatty conversion of bone marrow in females, which is more evident after menopause (Figure 2). There are also studies evaluating bone marrow fat with MRI-PDFF in patients with known or suspected NAFLD.[11, 38] It was demonstrated that there is also a close correlation between vertebral MRI-PDFF and age in NAFLD patients with slightly higher vertebral body MRI-PDFF in patients with type 2 diabetes mellitus.[11] Yu et al.[38] demonstrated a positive correlation between hepatic and lumbar MRI-PDFF in children with known or suspected NAFLD.

The differences in fat composition during specific treatments were also evaluated with MRI-PDFF by researchers.[34,39,40] Carmona et al.[39] demonstrated increased bone marrow MRI-PDFF in accordance with decreasing peripheral blood cell counts in patients receiving highly myelotoxic treatments for different malignancies. Martel et al.[34] showed altered bone marrow fat metabolism in the proximal femur by MRI-PDFF in patients using glucocorticoids. Dieckmeyer et al.[40] evaluated patients with breast cancer receiving combined aromatase inhibitor and bisphosphonate therapy and observed significantly increased PDFF after 12 months of treatment in comparison to patients receiving isolated aromatase inhibitor. These findings are promising to quantify temporal changes in MRI-PDFF of specific patient populations whose treatment efficacy monitoring is essential.

The role of MRI-PDFF was also evaluated in bone lesions, including both focal and inflammatory. Bray et al.[41] evaluated patients with sacroiliitis and observed that MRI-PDFF values were significantly lower in areas of edema compared to normal bone marrow. Increased MRI-PDFF values were observed in fat metaplasia areas of patients with known or suspected sacroiliitis.[41,42] Schmeel et al.[43] evaluated a total of 66 patients and observed that MRI-PDFF of non-neoplastic vertebral lesions is significantly higher than that of malignant lesions. In this study, they proposed a cutoff value of 6.4% to differentiate between benign and malignant lesions.[43] Kwack et al.[44] evaluated 126 patients with focal vertebral bone marrow lesions and observed statistically significantly lower MRI-PDFF values in metastasis and proposed a cutoff value of 9% for differentiation of metastasis from other benign lesions (Figure 3). Jung et al.[45] evaluated the role of MRI-PDFF in differentiating vertebral metastases from focal hematopoietic marrow depositions and observed improved diagnostic performance. Lee et al.[46] evaluated the role of MRI-PDFF in differentiating bone metastases from Schmorl nodes and observed that metasta-

Table 2. Defined cutoff values for MRI-PDFF in specific diseases affecting bone marrow

		Cutoff value (%)
Ergen et al.[13]	Healthy versus reduced bone mineralization level	<39.2
Schmeel et al.[43]	Benign versus malignant bone lesions	>6.4
Kwack et al.[44]	Benign vertebral lesions versus metastases	>9
Lee et al.[46]	Schmorl nodules versus metastases	>5.41

MRI-PDFF, magnetic resonance imaging-proton density fat fraction.

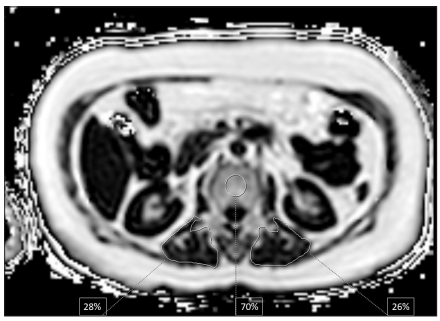

Figure 2. A 75-year-old woman with known osteoporosis with a measured fat fraction of 70% at the L3 vertebral body. Please also note the increased fat in the paraspinal muscles as 28% on the right and 26% on the left.

ses have lower fat fraction and fat fraction ratios than Schmorl nodes. Perez-Lopez et al.[47] evaluated bone metastases of prostate cancer and observed significantly lower fat fractions in bone metastasis in comparison with non-metastatic bone (Table 2). In this study, they also observed a significantly lower fat fraction in bone biopsies containing tumor in contrast with biopsies not containing tumor. Quantitative PDFF measurement of fat fraction in bone metastases may allow assessment of treatment response in prostate cancer patients.[47]

Muscle

The term myosteatosis, a possible concomitant component of sarcopenia, refers to fatty infiltration of the skeletal muscle, which is caused by several factors including aging, disuse, muscle injury, and hormonal dysfunction.[48] Myosteatosis is associated with loss of muscle mass and strength and increased mortality among the elderly.[48] Several studies investigated the effect of age and sex on fat accumulation in the skeletal muscle and demonstrated that men had lower muscle MRI-PDFF values in comparison to women.[49-51] There was also a significant correlation between muscle MRI-PDFF and age.[51] Burian et al.[52] demonstrated a correlation between abdominal muscle MRI-PDFF with age in both men and women and erector spinae muscle MRI-PDFF with age in women. In this study, they also observed a statistically significant association between age and abdominal muscle MRI-PDFF after adjusting BMI in women and concluded that myosteatosis is mainly correlated with age, but not with BMI in women.[52]

The relationship between muscle strength and MRI-PDFF was also evaluated. Schlaeger et al.[49] evaluated the relationship between the performance of erector spinae and psoas muscle strength with PDFF and cross-sectional area of the muscles in healthy individuals and observed that erector spinae muscle MRI-PDFF is negatively correlated with relative extension and flexion muscle strength. It remained as the only statistically significant predictor of relative extensor strength in multivariate regression models.[49] Similarly, Inhuber et al.[50] observed significant correlations between thigh muscle MRI-PDFF and relative maximum voluntary isometric contraction. Dieckmayer et al.[53] evaluated texture features of MRI-PDFF in paraspinal muscles and observed global Kurtosis of erector spinae muscle and BMI are statistically significant predictors of extension strength and global variance and skewness of psoas muscle are statistically significant predictors of flexion strength indicating that muscular function is related to muscle fat distribution. In contrast with the previous studies, Klupp et al.[54] did not find a correlation between paraspinal muscle strength and MRI-PDFF, but they found a correlation between diffusion tensor imaging parameters. The muscle MRI-PDFF and strength was also evaluated in different circumstances. Grimm et al.[55] evaluated thigh muscle area and MRI-PDFF in healthy subjects before and after training and observed that muscle area increases after training despite a significant decrease in muscle MRI-PDFF. Nguyen et al.[56] also evaluated MRI-PDFF of quadriceps muscle before and after a mountain ultramarathon race and observed a reduction in MRI-PDFF. Villagon et al.[57] evaluated the changes in fat distribution after fasting and observed an increase in muscle and spine bone marrow fat despite a decrease or no change in other regions of the body. Karampinos et al.[58] evaluated supraspinatus MRI-PDFF in patients 10 years after unilateral rotator cuff repair and observed that supraspinatus MRI-PDFF correlated significantly with Goutallier scores, more severe cartilage defects of the humerus and correlated negatively with isometric muscle strength. These studies demonstrated that MRI-PDFF can be used for demonstration of fatty infiltration of muscle as well as fat distribution in the muscle which is inversely related to the muscle strength.

There are also studies evaluating the relationship between muscle and bone marrow fat in the literature. Sollmann et al.[59] evaluated the relationship between paraspinal muscle and lumbar vertebrae MRI-PDFF in premenopausal and postmenopausal women and observed a significant correlation among them in postmenopausal women in comparison with premenopausal women. Zhao et al.[60] evaluated the relationship between paraspinal muscles and lumbar vertebrae MRI-PDFF in both women and men and observed lower paraspinal muscle MRI-PDFF values in patients with normal BMD in contrast with patients with osteopenia and osteoporosis (Figure 2). These two studies suggest a positive correlation between bone marrow and paraspinal muscle fat in patients with decreased BMD. Dieckmeyer et al.[61] evaluated the bone-muscle MRI-PDFF in the thigh and hip region in healthy volunteers and observed a weak correlation between only the MRI-PDFF of the quadriceps muscle and greater trochanter bone marrow. Burian et al.[62] did not find a correlation between bone marrow and muscle MRI-PDFF in sacral and lumbar spine regions in healthy volunteers. Although these conflicting results raise suspicion regarding the use of high levels of fat infiltration as a diagnostic or therapeutic tool for osteosarcopenia, it still maintains its importance for further exploration.

The studies also evaluated the role of MRI-PDFF in the assessment of fatty replacement in muscles in neuromuscular diseases such as Pompe disease and facio-scapulo-humeral dystrophy.[63-66] Horvath et al.[63] observed severe tongue and axial muscle group fat involvement with MRI-PDFF in

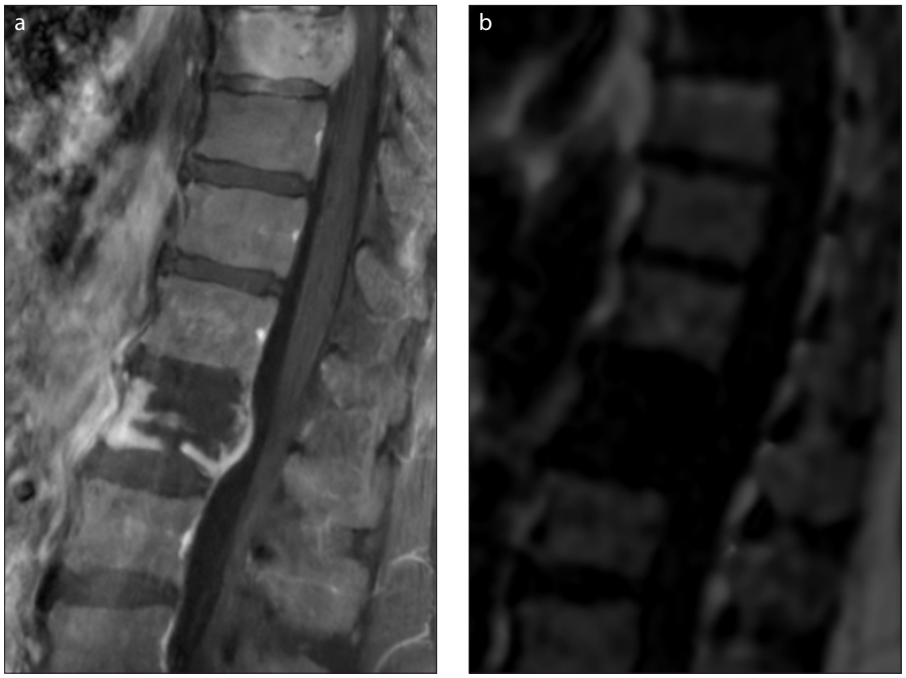

Figure 3. a, b. A 78-year-old male patient with primary lung cancer and bone metastasis at the T9 and L1 vertebral bodies with associated pathologic fracture at L1 vertebral body. Sagittal post-contrast T1-weighted image **(a)** demonstrates contrast enhancement of the metastasis with pathologic fracture at the L1 vertebra. Sagittal MRI-PDFF image **(b)** demonstrates low fat fraction in metastasis in contrast with normal vertebral bodies. Fat fraction of the metastasis at T9 vertebra was 0.5% and L1 vertebra was %2. However, the fat fraction of T12 vertebral body was measured as 40%.

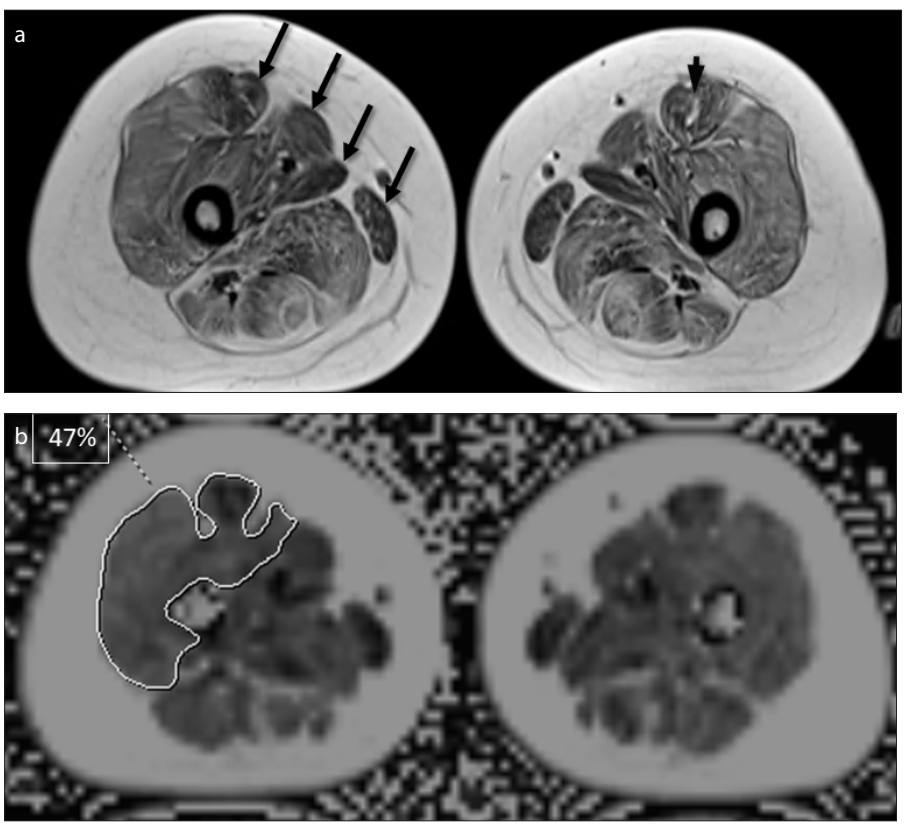

Figure 4. a, b. A 7-year-old female patient with Ullrich congenital muscular dystrophy. Axial T1-weighted image **(a)** shows diffuse fatty replacement of the thigh muscles with relative sparing of rectus femoris except its central area (prominent at left thigh, *arrowhead*), sartorius, adductor longus and gracilis muscles (*arrows* at right thigh). Quantification of the fat fraction with MRI-PDFF **(b)** demonstrates 47% fat in the right quadriceps femoris muscle.

patients with late-onset Pompe disease (LOPD) and proposed that whole-body MRI provides more detailed data than physical examination. Khan et al.[64] showed muscle strength and functional testing in patients with LOPD are correlated with MRI-PDFF and supposed that MRI-PDFF can be used for assessment of the severity of muscle disease and follow-up. Fernandez et al.[65] evaluated muscle fat infiltration with MRI-PDFF in children with infantile Pompe disease (IPD) and pediatric LOPD and observed that patients with IPD had higher PDFF values in comparison with LOPD patients despite younger age in IPD population. Leporq et al.[66] evaluated seven patients with facio-scapulo-humeral dystrophy and higher fatty infiltration was observed in muscles despite a normal appearance of the muscle. Stouge et al.[67] evaluated patients with diabetes with and without diabetic polyneuropathy in comparison with healthy controls and demonstrated higher fat fraction in lower extremity muscles in patients with diabetic polyneuropathy. MRI-PDFF allows demonstration and quantification of fatty replacement in muscles in neuromuscular diseases which may be helpful in both diagnosis and evaluation of treatment response (Figure 4).

The effects of hormonal disorders on myosteatosis with MRI-PDFF were also evaluated by several researchers. Sollman et al.[59] observed significantly higher paraspinal muscle PDFF in patients with postmenopausal women compared to premenopausal women. Kiefer et al.[68] evaluated abdominal muscle MRI-PDFF in patients with prediabetes and diabetes as well as healthy controls and observed statistically higher MRI-PDFF in patients with prediabetes and diabetes in contrast with healthy controls. Oguz et al.[27] evaluated patients with the lean PCOS and observed lower paraspinal muscle and lumbar MRI-PDFF values in the patient population compared to healthy individuals.

Miscellaneous

There are also different studies evaluating the usage of MRI-PDFF in different organs and tissues. Franz et al.[69] evaluated supraclavicular and gluteal region adipose tissue MRI-PDFF and observed a close correlation with VAT-SAT volume and moderate correlation with liver MRI-PDFF. Hong et al.[70] evaluated the role of MRI-PDFF in the assessment of spleen fat in comparison

with magnetic resonance spectroscopy and observed poor agreement between two methods with higher fat fraction values with MRI-PDFF which can be artifactual. Idilman et al.[71] evaluated R2* values of the spleen in patients with transfusion-related iron overload and observed no correlation with R2* values of liver, pancreas, renal cortex, and vertebral bone marrow with MRI-PDFF. However, in this study, they demonstrated positive correlations between liver R2* and pancreas-renal cortex R2* as well as pancreas R2* and renal cortex R2*. Idilman et al.[11] evaluated the relationship between renal cortex and sinus MRI-PDFF with liver, pancreas and vertebra MRI-PDFF and observed a correlation between renal sinus PDFF and pancreas PDFF. In another study, Notohamiprodjo et al.[72] demonstrated renal sinus fat volume is higher in prediabetic and diabetic subjects and also associated with VAT.

Guo et al.[73] evaluated testis and epididymis fat fraction with MRI-PDFF in different age groups and observed increased fat deposition with age and a reduction of fat fraction after ejaculation. Li et al.[74] evaluated the utility of testicular fat deposition in determining and monitoring testicular infertility and demonstrated that testicular fat deposition determined by MRI-PDFF is more specific than testicular volume for diagnosis of male infertility and suggested that it can also be used for monitoring infertility.

Conclusion

MRI-PDFF can be used for demonstration and quantification of fat in various organs and tissues as well as liver, which may show the effect of both in several diseases. Pancreas MRI-PDFF is shown to be related to various metabolic, inflammatory, and neoplastic diseases. Bone marrow MRI-PDFF allows quantification of fatty replacement which is related to loss of bone mass. It is also useful for the differentiation of benign fractures from malignancy-associated ones. Muscle MRI-PDFF can be used for the determination of muscle strength and also muscle involvement in neuromuscular diseases. We believe that further studies will expand the utilization of MRI-PDFF in various organs and tissues and will help the understanding of fat metabolism.

Conflict of interest disclosure

The authors declared no conflicts of interest.

References

1. Yokoo T, Bydder M, Hamilton G, et al. Nonalcoholic fatty liver disease: diagnostic and fat-grading accuracy of low-flip-angle multiecho gradient-recalled-echo MR imaging at 1.5 T. *Radiology.* 2009;251(1):67-76. [Crossref]
2. Reeder SB, Robson PM, Yu H, et al. Quantification of hepatic steatosis with MRI: the effects of accurate fat spectral modeling. *J Magn Reson Imaging.* 2009;29(6):1332-1339. [Crossref]
3. Reeder SB, Cruite I, Hamilton G, Sirlin CB. Quantitative assessment of liver fat with magnetic resonance imaging and spectroscopy. *J Magn Reson Imaging.* 2011;34(4):729-749. [Crossref]
4. Permutt Z, Le TA, Peterson MR, Seki E, Brenner DA, Sirlin C, Loomba R. Correlation between liver histology and novel magnetic resonance imaging in adult patients with non-alcoholic fatty liver disease - MRI accurately quantifies hepatic steatosis in NAFLD. *Aliment Pharmacol Ther.* 2012;36(1):22-29. [Crossref]
5. Tang A, Tan J, Sun M, Hamilton G, Bydder M, Wolfson T, Gamst AC, Middleton M, Brunt EM, Loomba R, Lavine JE, Schwimmer JB, Sirlin CB. Nonalcoholic fatty liver disease: MR imaging of liver proton density fat fraction to assess hepatic steatosis. *Radiology.* 2013;267(2):422-431. [Crossref]
6. Idilman IS, Aniktar H, Idilman R, et al. Hepatic steatosis: quantification by proton density fat fraction with MR imaging versus liver biopsy. *Radiology.* 2013;267(3):767-775. [Crossref]
7. Idilman IS, Keskin O, Elhan AH, Idilman R, Karcaaltincaba M. Impact of sequential proton density fat fraction for quantification of hepatic steatosis in nonalcoholic fatty liver disease. *Scand J Gastroenterol.* 2014;49(5):617-624. [Crossref]
8. Ajmera V, Park CC, Caussy C, et al. Magnetic resonance imaging proton density fat fraction associates with progression of fibrosis in patients with nonalcoholic fatty liver disease. *Gastroenterology.* 2018;155(2):307-310.e2. [Crossref]
9. Caussy C, Reeder SB, Sirlin CB, Loomba R. Noninvasive, quantitative assessment of liver fat by MRI-PDFF as an endpoint in NASH trials. *Hepatology.* 2018;68(2):763-772. [Crossref]
10. Schawkat K, Eshmuminov D, Lenggenhager D, et al. Preoperative evaluation of pancreatic fibrosis and lipomatosis: correlation of magnetic resonance findings with histology using magnetization transfer imaging and multigradient echo magnetic resonance imaging. *Invest Radiol.* 2018;53(12):720-727. [Crossref]
11. Idilman IS, Tuzun A, Savas B, et al. Quantification of liver, pancreas, kidney, and vertebral body MRI-PDFF in non-alcoholic fatty liver disease. *Abdom Imaging.* 2015;40(6):1512-1519. [Crossref]
12. Kühn JP, Hernando D, Meffert PJ, et al. Proton-density fat fraction and simultaneous R2* estimation as an MRI tool for assessment of osteoporosis. *Eur Radiol.* 2013;23(12):3432-3439. [Crossref]
13. Ergen FB, Gulal G, Yildiz AE, Celik A, Karakaya J, Aydingoz U. Fat fraction estimation of the vertebrae in females using the T2*-IDEAL technique in detection of reduced bone mineralization level: comparison with bone mineral densitometry. *J Comput Assist Tomogr.* 2014;38(2):320-324. [Crossref]
14. Li GW, Xu Z, Chen QW, et al. Quantitative evaluation of vertebral marrow adipose tissue in postmenopausal female using MRI chemical shift-based water-fat separation. *Clin Radiol.* 2014;69(3):254-262. [Crossref]
15. Kühn JP, Berthold F, Mayerle J, et al. Pancreatic steatosis demonstrated at MR imaging in the general population: clinical relevance. *Radiology.* 2015;276(1):129-136. [Crossref]
16. Patel NS, Peterson MR, Brenner DA, Heba E, Sirlin C, Loomba R. Association between novel MRI-estimated pancreatic fat and liver histology-determined steatosis and fibrosis in non-alcoholic fatty liver disease. *Aliment Pharmacol Ther.* 2013;37(6):630-639. [Crossref]
17. Kato S, Iwasaki A, Kurita Y, et al. Three-dimensional analysis of pancreatic fat by fat-water magnetic resonance imaging provides detailed characterization of pancreatic steatosis with improved reproducibility. *PLoS One.* 2019;14(12):e0224921. [Crossref]
18. Idilman IS, Low HM, Gidener T, et al. Association between visceral adipose tissue and non-alcoholic steatohepatitis histology in patients with known or suspected non-alcoholic fatty liver disease. *J Clin Med.* 2021;10(12):2565. [Crossref]
19. Vieira J, Amorim J, Martí-Bonmatí L, Alberich-Bayarri Á, França M. Quantifying steatosis in the liver and pancreas with MRI in patient with chronic liver disease. *Radiologia.* 2020;62(3):222-228. [Crossref]
20. Patel NS, Peterson MR, Lin GY, et al. Insulin resistance increases MRI-estimated pancreatic fat in nonalcoholic fatty liver disease and normal controls. *Gastroenterol Res Pract.* 2013;2013:498296. [Crossref]
21. Sarma MK, Saucedo A, Darwin CH, et al. Noninvasive assessment of abdominal adipose tissues and quantification of hepatic and pancreatic fat fractions in type 2 diabetes mellitus. Magn Reson Imaging. 2020;72:95-102. [Crossref]
22. Trout AT, Hunte DE, Mouzaki M, et al. Relationship between abdominal fat stores and liver fat, pancreatic fat, and metabolic comorbidities in a pediatric population with non-alcoholic fatty liver disease. *Abdom Radiol (NY).* 2019;44(9):3107-3114. [Crossref]
23. Chiyanika C, Chan DFY, Hui SCN, et al. The relationship between pancreas steatosis and the risk of metabolic syndrome and insulin resistance in Chinese adolescents with concurrent obesity and non-alcoholic fatty liver disease. *Pediatr Obes.* 2020;15(9):e12653. [Crossref]
24. Covarrubias Y, Fowler KJ, Mamidipalli A, et al. Pilot study on longitudinal change in pancreatic proton density fat fraction during a weight-loss surgery program in adults with obesity. *J Magn Reson Imaging.* 2019;50(4):1092-1102. [Crossref]
25. Singh RG, Cervantes A, Kim JU, et al. Intrapancreatic fat deposition and visceral fat volume are associated with the presence of diabetes after acute pancreatitis. *Am J Physiol Gastrointest Liver Physiol.* 2019;316(6):G806-G815. [Crossref]
26. Lind L, Salihovic S, Risérus U, et al. The plasma metabolomic profile is differently associated with liver fat, visceral adipose tissue, and pancreatic fat. *J Clin Endocrinol Metab.* 2020:dgaa693. [Crossref]

27. Oguz SH, İdilman I, Helvaci N, et al. Tissue fat quantification by magnetic resonance imaging: proton density fat fraction in polycystic ovary syndrome. *Reprod Biomed Online.* 2020;41(2):329-334. [Crossref]
28. Singh RG, Yoon HD, Wu LM, Lu J, Plank LD, Petrov MS. Ectopic fat accumulation in the pancreas and its clinical relevance: A systematic review, meta-analysis, and meta-regression. *Metabolism.* 2017;69:1-13. [Crossref]
29. Kromrey ML, Friedrich N, Hoffmann RT, et al. Pancreatic steatosis is associated with impaired exocrine pancreatic function. *Invest Radiol.* 2019;54(7):403-408. [Crossref]
30. Boga S, Koksal AR, Sen I, et al. Liver and pancreas: 'Castor and Pollux' regarding the relationship between hepatic steatosis and pancreas exocrine insufficiency. *Pancreatology.* 2020;20(5):880-886. [Crossref]
31. Tahtacı M, Algın O, Karakan T, et al. Can pancreatic steatosis affect exocrine functions of pancreas? *Turk J Gastroenterol.* 2018;29(5):588-594. [Crossref]
32. Fukui H, Hori M, Fukuda Y, et al. Evaluation of fatty pancreas by proton density fat fraction using 3-T magnetic resonance imaging and its association with pancreatic cancer. *Eur J Radiol.* 2019;118:25-31. [Crossref]
33. Guo Y, Chen Y, Zhang X, et al. Magnetic susceptibility and fat content in the lumbar spine of postmenopausal women with varying bone mineral density. *J Magn Reson Imaging.* 2019;49(4):1020-1028. [Crossref]
34. Martel D, Leporq B, Saxena A, et al. 3T chemical shift-encoded MRI: Detection of altered proximal femur marrow adipose tissue composition in glucocorticoid users and validation with magnetic resonance spectroscopy. *J Magn Reson Imaging.* 2019;50(2):490-496. [Crossref]
35. Dunnill MS, Anderson JA, Whitehead R. Quantitative histological studies on age changes in bone. *J Pathol Bacteriol.* 1967;94(2):275-291. [Crossref]
36. Verma S, Rajaratnam JH, Denton J, Hoyland JA, Byers RJ. Adipocytic proportion of bone marrow is inversely related to bone formation in osteoporosis. *J Clin Pathol.* 2002;55(9):693-698. [Crossref]
37. Baum T, Rohrmeier A, Syväri J, et al. Anatomical variation of age-related changes in vertebral bone marrow composition using chemical shift encoding-based water-fat magnetic resonance imaging. *Front Endocrinol (Lausanne).* 2018;9:141. [Crossref]
38. Yu NY, Wolfson T, Middleton MS, et al. Bone marrow fat content is correlated with hepatic fat content in paediatric non-alcoholic fatty liver disease. *Clin Radiol.* 2017;72(5):425.e9-425.e14. [Crossref]
39. Carmona R, Pritz J, Bydder M, et al. Fat composition changes in bone marrow during chemotherapy and radiation therapy. *Int J Radiat Oncol Biol Phys.* 2014;90(1):155-163. [Crossref]
40. Dieckmeyer M, Ruschke S, Rohrmeier A, et al. Vertebral bone marrow fat fraction changes in postmenopausal women with breast cancer receiving combined aromatase inhibitor and bisphosphonate therapy. *BMC Musculoskelet Disord.* 2019;20(1):515. [Crossref]
41. Bray TJP, Bainbridge A, Punwani S, Ioannou Y, Hall-Craggs MA. Simultaneous quantification of bone edema/adiposity and structure in inflamed bone using chemical shift-encoded MRI in spondyloarthritis. *Magn Reson Med.* 2018;79(2):1031-1042. [Crossref]
42. Bray TJP, Sakai N, Dudek A, et al. Histographic analysis of oedema and fat in inflamed bone marrow based on quantitative MRI. *Eur Radiol.* 2020;30(9):5099-5109. [Crossref]
43. Schmeel FC, Luetkens JA, Wagenhäuser PJ, et al. Proton density fat fraction (PDFF) MRI for differentiation of benign and malignant vertebral lesions. *Eur Radiol.* 2018;28(6):2397-2405. [Crossref]
44. Kwack KS, Lee HD, Jeon SW, Lee HY, Park S. Comparison of proton density fat fraction, simultaneous R2*, and apparent diffusion coefficient for assessment of focal vertebral bone marrow lesions. *Clin Radiol.* 2020;75(2):123-130. [Crossref]
45. Jung Y, Jeon SW, Kwack KS, Yun JS, Lee HD, Park S. Differentiation of vertebral metastases from focal hematopoietic marrow depositions on MRI: added value of proton density fat fraction. *AJR Am J Roentgenol.* 2021;6:1-8. [Crossref]
46. Lee JH, Park S. Differentiation of Schmorl nodes from bone metastases of the spine: use of apparent diffusion coefficient derived from DWI and fat fraction derived from a Dixon sequence. *AJR Am J Roentgenol.* 2019;213(5):W228-W235. [Crossref]
47. Perez-Lopez R, Nava Rodrigues D, Figueiredo I, et al. Multiparametric magnetic resonance imaging of prostate cancer bone disease: correlation with bone biopsy histological and molecular features. Invest Radiol. 2018;53(2):96-102. [Crossref]
48. Hamrick MW, McGee-Lawrence ME, Frechette DM. Fatty infiltration of skeletal muscle: mechanisms and comparisons with bone marrow adiposity. *Front Endocrinol (Lausanne).* 2016;7:69. [Crossref]
49. Schlaeger S, Inhuber S, Rohrmeier A, et al. Association of paraspinal muscle water-fat MRI-based measurements with isometric strength measurements. *Eur Radiol.* 2019;29(2):599-608. [Crossref]
50. Inhuber S, Sollmann N, Schlaeger S, et al. Associations of thigh muscle fat infiltration with isometric strength measurements based on chemical shift encoding-based water-fat magnetic resonance imaging. *Eur Radiol Exp.* 2019;3(1):45. [Crossref]
51. Burian E, Franz D, Greve T, et al. Age- and gender-related variations of cervical muscle composition using chemical shift encoding-based water-fat MRI. *Eur J Radiol.* 2020 Apr;125:108904. [Crossref]
52. Burian E, Syväri J, Holzapfel C, et al. Gender- and age-related changes in trunk muscle composition using chemical shift encoding-based water-fat MRI. *Nutrients.* 2018;10(12):1972. [Crossref]
53. Dieckmeyer M, Inhuber S, Schlaeger S, et al. Texture features of proton density fat fraction maps from chemical shift encoding-based MRI predict paraspinal muscle strength. *Diagnostics (Basel).* 2021;11(2):239. [Crossref]
54. Klupp E, Cervantes B, Schlaeger S, et al. Paraspinal muscle DTI metrics predict muscle strength. *J Magn Reson Imaging.* 2019;50(3):816-823. [Crossref]
55. Grimm A, Nickel MD, Chaudry O, et al. Feasibility of Dixon magnetic resonance imaging to quantify effects of physical training on muscle composition-A pilot study in young and healthy men. *Eur J Radiol.* 2019;114:160-166. [Crossref]
56. Nguyen HT, Grenier T, Leporq B, et al. Quantitative magnetic resonance imaging assessment of the quadriceps changes during an extreme mountain ultramarathon. *Med Sci Sports Exerc.* 2021;53(4):869-881. [Crossref]
57. Viallon M, Leporq B, Drinda S, et al. Chemical-shift-encoded magnetic resonance imaging and spectroscopy to reveal immediate and long-term multi-organs composition changes of a 14-days periodic fasting intervention: a technological and case report. *Front Nutr.* 2019;6:5. [Crossref]
58. Karampinos DC, Holwein C, Buchmann S, et al. Proton density fat-fraction of rotator cuff muscles is associated with isometric strength 10 years after rotator cuff repair: a quantitative magnetic resonance imaging study of the shoulder. *Am J Sports Med.* 2017;45(9):1990-1999. [Crossref]
59. Sollmann N, Dieckmeyer M, Schlaeger S, et al. Associations between lumbar vertebral bone marrow and paraspinal muscle fat compositions-an investigation by chemical shift encoding-based water-fat MRI. *Front Endocrinol (Lausanne).* 2018;9:563. [Crossref]
60. Zhao Y, Huang M, Serrano Sosa M, et al. Fatty infiltration of paraspinal muscles is associated with bone mineral density of the lumbar spine. *Arch Osteoporos.* 2019;14(1):99. [Crossref]
61. Dieckmeyer M, Zoffl F, Grundl L, et al. Association of quadriceps muscle, gluteal muscle, and femoral bone marrow composition using chemical shift encoding-based water-fat MRI: a preliminary study in healthy young volunteers. *Eur Radiol Exp.* 2020;4(1):35. [Crossref]
62. Burian E, Syväri J, Dieckmeyer M, et al. Age- and BMI-related variations of fat distribution in sacral and lumbar bone marrow and their association with local muscle fat content. *Sci Rep.* 2020;10(1):9686. [Crossref]
63. Horvath JJ, Austin SL, Case LE, et al. Correlation between quantitative whole-body muscle magnetic resonance imaging and clinical muscle weakness in Pompe disease. *Muscle Nerve.* 2015;51(5):722-730. [Crossref]
64. Khan AA, Boggs T, Bowling M, et al. Whole-body magnetic resonance imaging in late-onset Pompe disease: Clinical utility and correlation with functional measures. J Inherit Metab Dis. 2020;43(3):549-557. [Crossref]
65. Fernandes SA, Khan AA, Boggs T, et al. Quantitative whole-body magnetic resonance imaging in children with Pompe disease: Clinical tools to evaluate severity of muscle disease. *JIMD Rep.* 2020;57(1):94-101. [Crossref]
66. Leporq B, Le Troter A, Le Fur Y, et al. Combined quantification of fatty infiltration, T1-relaxation times and T2*-relaxation times in normal-appearing skeletal muscle of controls and dystrophic patients. *MAGMA.* 2017;30(4):407-415. [Crossref]
67. Stouge A, Khan KS, Kristensen AG, et al. MRI of skeletal muscles in participants with type 2 diabetes with or without diabetic polyneuropathy. *Radiology.* 2020;297(3):608-619. [Crossref]
68. Kiefer LS, Fabian J, Rospleszcz S, et al. Assessment of the degree of abdominal myosteatosis by magnetic resonance imaging in subjects with diabetes, prediabetes and healthy controls from the general population. *Eur J Radiol.* 2018;105:261-268. [Crossref]

69. Franz D, Weidlich D, Freitag F, et al. Association of proton density fat fraction in adipose tissue with imaging-based and anthropometric obesity markers in adults. *Int J Obes (Lond).* 2018;42(2):175-182. [Crossref]
70. Hong CW, Hamilton G, Hooker C, et al. Measurement of spleen fat on MRI-proton density fat fraction arises from reconstruction of noise. *Abdom Radiol (NY).* 2019;44(10):3295-3303. [Crossref]
71. İdilman İS, Gümrük F, Haliloğlu M, Karçaaltıncaba M. The feasibility of magnetic resonance imaging for quantification of liver, pancreas, spleen, vertebral bone marrow, and renal cortex R2* and proton density fat fraction in transfusion-related iron overload. *Turk J Haematol.* 2016;33(1):21-27. [Crossref]
72. Notohamiprodjo M, Goepfert M, Will S, et al. Renal and renal sinus fat volumes as quantified by magnetic resonance imaging in subjects with prediabetes, diabetes, and normal glucose tolerance. *PLoS One.* 2020;15(2):e0216635. [Crossref]
73. Guo RM, Zhao RZ, Zhang J, et al. Quantification of fat deposition in the testis and epididymis using mDIXON Quant sequence: correlation with age and ejaculation. *Abdom Radiol (NY).* 2019;44(4):1528-1534. [Crossref]
74. Li QL, Yang F, Zhou WY, et al. Quantification of testicular fat deposition in the evaluation of middle-aged overweight male infertility. *MAGMA.* 2020;33(3):377-384. [Crossref]